ACS EARTH AND SPACE CHEMISTRY

http://pubs.acs.org/journal/aesccq

Article

Assessing the Difference in the Effects of NO_x on the Photooxidation Mechanisms of Isomeric Compounds of α-Pinene and Δ^3-Carene

Zhaoyan Zhang,[#] Xiangyu Zang,[#] Yingqi Zhao, Ya Zhao, Hua Xie, Gang Li,[*] Ling Jiang,[*] and Xueming Yang

Cite This: *ACS Earth Space Chem.* 2024, 8, 1668−1679

Read Online

ACCESS | Metrics & More | Article Recommendations | Supporting Information

ABSTRACT: Elucidating the difference between the photooxidation mechanisms of isomeric volatile organic compounds (VOCs) by anthropogenic pollutants helps to unravel the structural dependence of VOCs on the formation of secondary organic aerosols (SOAs). Herein, the effects of NO_x (NO and NO_2) on the SOA formation from the photooxidation of isomeric monoterpenes of α-pinene and Δ^3-carene were compared by a series of experimental and theoretical studies. For both the α-pinene and the Δ^3-carene systems, the increase of NO and NO_2 concentration ([NO] and [NO_2]) first enhances and then suppresses the particle number concentration but enhances the particle size growth (except for the photooxidation of Δ^3-carene with NO). The increase of [NO_x] first promotes and then suppresses the SOA yields of α-pinene. In particular, the increase of [NO] suppresses the SOA yields of Δ^3-carene, whereas the increase of [NO_2] promotes the SOA yields of Δ^3-carene. These findings imply that the "rate effect" (a faster oxidation rate leads to a higher SOA yield) of photooxidation for Δ^3-carene with NO_2 may be more pronounced than that of α-pinene. The number of SOA components with higher O/C in the Δ^3-carene system is larger than that in the α-pinene system, which could be rationalized that the bond tension of the three-membered ring structure of Δ^3-carene is larger than that of the four-membered ring of α-pinene. The present findings serve as a model for clarifying the effects of NO_x on the SOA formation of VOCs with the same chemical formula and stimulate systematic studies on a broad class of isomeric VOCs toward the improvement of SOA models.

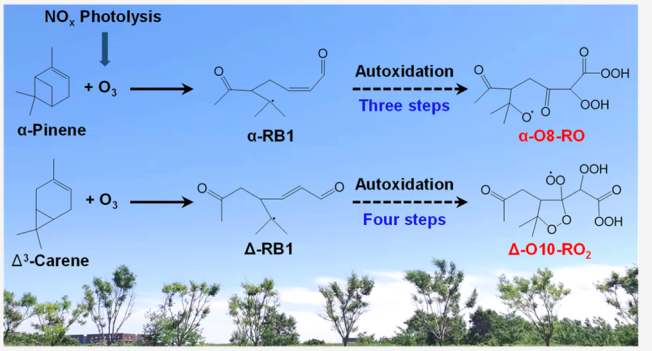

KEYWORDS: *secondary organic aerosol, anthropogenic−biogenic interactions, photooxidation mechanism, α-pinene, Δ-carene*

1. INTRODUCTION

Secondary organic aerosols (SOAs) are condensed-phase matters, which are mainly formed by the reactions between volatile organic compounds (VOCs) and atmospheric oxidants. SOAs contribute significantly to the global aerosol content and have serious impacts on the atmospheric environment.[1−4] In particular, biogenic VOCs (BVOCs) serve as the key precursors of SOAs.[1] Monoterpene emissions are estimated to exceed 100 Tg/yr globally, accounting for approximately 10% of BVOC emissions, and the SOA formed from monoterpene could contribute 50% or larger to total SOA in some forested regions.[5,6] Numerous studies have identified the monoterpene-derived SOAs as potentially important contributors to the particles.[7−10] Since the α-pinene and β-pinene compounds are typically the most abundant bioemitted monoterpenes,[5] their SOA formation mechanisms have been extensively studied.[11−14] Among other monoterpenes, Δ^3-carene accounts for almost the same proportion as α-pinene in the VOCs released by Scots pine.[15]

α-Pinene and Δ^3-carene are isomeric compounds ($C_{10}H_{16}$) (Scheme 1), both of which consist of six-membered carbon rings, endocyclic double bond, and methyl substituents on the skeleton. The main structural difference of α-pinene and Δ^3-carene lies in the secondary ring structure, in which α-pinene

Scheme 1. Structures of α-Pinene and Δ^3-Carene

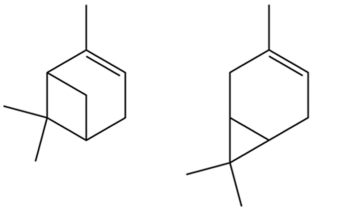

Received: May 30, 2024
Revised: June 26, 2024
Accepted: June 27, 2024
Published: July 11, 2024

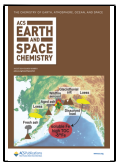

Table 1. Experimental Conditions of α-Pinene and Δ^3-Carene Photooxidation under Different NO and NO_2 Concentrations[a]

	$[VOC]_0$ (ppb)	$[NO_2]_0$ (ppb)	$[NO]_0$ (ppb)	$[VOC]_0/[NO_x]_0$	ΔROG (ppb)	ΔM ($\mu g/m^3$)	SOA yield (%)
α-pinene	337	50	1.4	6.6	337	375.8	16.4
	385	112	4	3.3	385	523.9	23.4
	358	201	5	1.7	358	820.6	36.9
	376	296	12	1.2	376	1256.2	54.9
	364	402	26	0.9	364	240.0	10.9
	374	24	55	4.7	374	310.3	13.7
	354	8	118	2.8	354	447.5	20.8
	380	3	213	1.8	380	580.9	25.1
	362	15	302	1.1	362	784.9	35.6
	475	47	404	1.1	475	141.7	4.9
Δ^3-carene	414	49	3	8.0	414	371.6	14.8
	338	101	7	3.1	338	308.0	15.0
	380	207	10	1.8	380	519.9	22.5
	383	300	9	1.2	383	627.5	26.9
	442	396	14	1.1	442	523.7	19.5
	335	28	58	3.9	335	292.0	14.4
	352	37	111	2.4	352	129.0	6.0
	388	13	204	1.8	388	127.0	5.4
	373	15	291	1.2	373	60.0	2.6
	380	59	388	0.9	380		

[a] $[X]_0$: the initial concentration of the species X; ΔROG: the amount of reacted organic gas; ΔM: the mass concentration of formed SOA.

has a four-membered carbocycle while Δ^3-carene consists of a three-membered carbocycle. The SOA formation mechanisms of α-pinene and Δ^3-carene were proposed to be similar because of their structural similarity and ozonolysis pathways.[16−18] The study conducted in a laminar flow reactor revealed that the ozonolysis of α-pinene and Δ^3-carene exhibited a similar temperature dependence on the particle number concentrations and particle mass concentrations.[19] Strikingly, the ozonolysis of Δ^3-carene was found to favor larger particle mass and higher SOA than that of α-pinene, and the diversity of product distribution in the Δ^3-carene-derived SOA was much less than that in the α-pinene-derived SOA.[20] Under similar OH-dominated conditions, the SOA yield of Δ^3-carene photooxidation was higher than that of the α-pinene photooxidation.[21] Thus, more detailed studies on the reactions between anthropogenic pollutants and isomeric compounds of monoterpenes are expected to uncover the multifaceted mechanisms of SOA formation and refine the representative VOCs in the air quality models.

The interactions of anthropogenic pollutant NO_x (NO and NO_2) with RO_2 intriguingly affect the SOA formation and product species.[22] The suppression effect of high NO_x concentrations ($[NO_x]$) on the SOA yield has long been an important issue.[11,22−25] It could be rationalized that the volatility of nitrate products generated from the RO_2 + NO reaction is higher than that of the hydroperoxide products generated from the RO_2 + HO_2 reaction.[11,22,23] On the other hand, the absence of particle surfaces for condensing organic compounds and the vapor wall loss on the mass yield also contribute to the NO_x suppression effect.[25] The H/C value of α-pinene-derived SOA at high $[NO_x]$ is lower than that at low $[NO_x]$.[25] The $[NO_x]$ dependence study indicated that the NO_x suppression effect is mainly reflected in the impact on the OH concentration ([OH]).[14] The study indicated that OH was formed in two ways: the photolysis of ozone stemmed from NO_x and the reaction of NO + HO_2 → NO_2 + OH; the maximum [OH] was estimated to be ∼3.8 × 10^7 molecules cm^{-3} (∼1.6 ppt).[26] The study also revealed notable distinctions in the photooxidation outcomes of VOC and NO_x when NO and NO_2 were individually considered as the main components of NO_x.[14] Under the dark condition with different $[NO_2]$, the α-pinene and Δ^3-carene ozonolysis showed different changes in the particle number concentrations and particle mass concentrations and the significance of NO_3-initiated SOA formation.[27] The alkoxy radicals' fates after the RO_2 + NO reactions may be different for the α-pinene and Δ^3-carene systems.[28] Thus far, limited information is available to the differences between the SOA formation mechanisms of α-pinene and Δ^3-carene photooxidations with NO_x.

In this study, we investigated the effects of NO and NO_2 on the photooxidation mechanisms of isomeric monoterpenes of α-pinene and Δ^3-carene by a series of experimental and theoretical studies. The changes in [NO] and $[NO_2]$ are found to have remarkably different effects on the photooxidation mechanisms of the α-pinene and Δ^3-carene systems. Especially, the Δ^3-carene-derived SOAs have more high-oxygen-content products than the α-pinene-derived SOAs. The present findings provide new insights into the interaction mechanisms of isomeric VOCs with anthropogenic pollutants.

2. EXPERIMENTAL AND THEORETICAL METHODS

The photooxidation experiments were carried out in a smog chamber reported previously,[29] containing a 2 m^3 cylindrical Teflon reactor. The present experimental and theoretical methods are detailly given in the Supporting information (SI) and briefly described below. The 40 black tube lamps (F40BLB) were used to trigger photochemical reactions. Relative humidity and the temperature of the reactor were ∼2.0% and 23 ± 1.3 °C, respectively. The α-pinene and Δ^3-carene liquid samples were brought into the Teflon reactor by the zero gas at 60 °C. The concentrations of VOCs, $[NO_x]$, and $[O_3]$ were measured by Model 42i, Model 49i, and proton-transfer reaction mass spectrometer, respectively. The particle size distributions, particle number concentrations, and

https://doi.org/10.1021/acsearthspacechem.4c00159
ACS Earth Space Chem. 2024, 8, 1668−1679

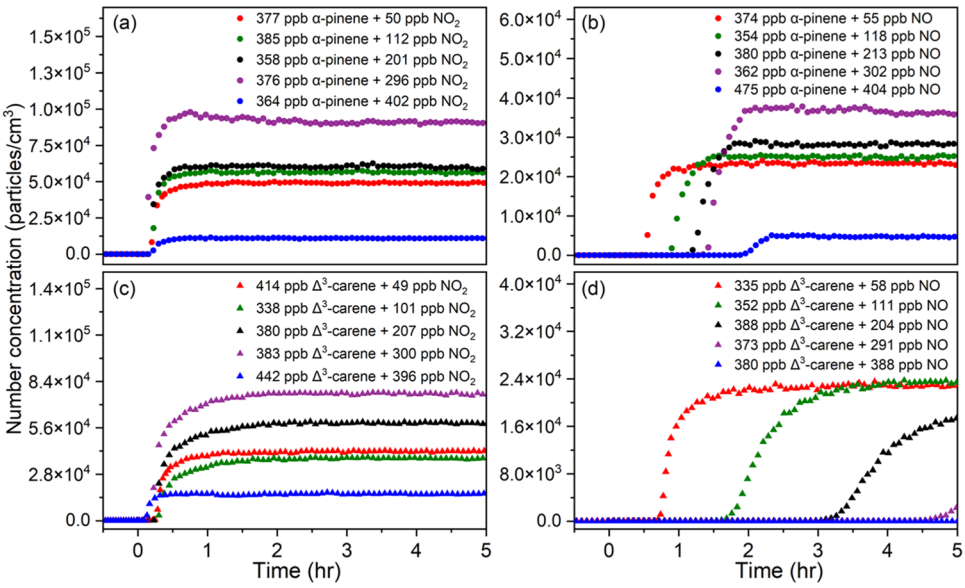

Figure 1. Particle number concentrations in the photooxidation of α-pinene (a, b) and Δ^3-carene (c, d) under different NO and NO_2 concentrations. (d) The maximum particle number concentration under the condition of 373 ppb Δ^3-carene +291 ppb NO is 1.4×10^4 particles/cm^3.

particle mass concentrations were measured by a scanning mobility particle sizer spectrometer.

Initial concentrations of reactants were recorded after the reactants were injected, mixed until uniform, and then allowed to stand for 30 min. The wall losses for particle number concentrations and particle mass concentrations were corrected.[12] Owing to the difficulty in the accurate assessment of gas-wall losses of gas phase products in the smog chamber studies,[30] the wall losses of α-pinene, Δ^3-carene, and semivolatile/low-volatile products were not considered in this study. Losses in the sample line were also not considered. Thus, the value of SOA yield would be underestimated.

The end time of the photooxidation reaction was marked when the mass concentration of particles no longer showed a significant increase. Subsequently, particle samples were collected using a quartz filter membrane (Pall, 47 mm) by 30 min. Prior to usage, all quartz filter membranes were baked at 600 °C for at least 5 h to eliminate the possibly adsorbed organic matter. Based on the previous studies,[20,31] particle samples were ultrasonically extracted with the methanol solvent (TCI, HPLC grade) for 1 h. The filtered liquid was then purged with high-purity nitrogen (99.999%) until it was almost dry. The residue was dissolved in 500 μL of methanol and prepared for detection in an Orbitrap Fusion Lumos Tribrid mass spectrometer with negative ion mode. Furthermore, a second extraction was performed for one of the filters. Compared with the mass spectra of the first extraction, most of peaks disappeared in the mass spectra of the second extraction (Figure S1). These results indicated that the particle samples were almost completely dissolved in the solvent. During the detection of SOA samples, the mass spectrometer was configured with a resolution of 240 000.

Quantum chemical calculations for geometric optimization and reaction pathways of the products were carried out at the ωB97XD/def2-TZVP level of theory with the Gaussian 16 program package.[32]

3. RESULTS AND DISCUSSION

3.1. Effects of NO_x on the Particle Number Concentration and Size Distribution. The α-pinene and Δ^3-carene photooxidation experiments were explored with different [NO] and [NO_2] (Table 1), respectively. As shown in Figure 1, for the α-pinene photooxidation, the particle number concentration in the ~50 ppb NO_2 condition (red dot in Figure 1a) is found to be higher than that in the ~50 ppb NO condition (red dot in Figure 1b). Similar results are also observed in a higher [NO] and [NO_2] condition (~400 ppb). These findings indicate that the SOA formation from the α-pinene photooxidation by NO_2 is more favorable than that by NO. This holds true for the Δ^3-carene photooxidation (Figure 1c,d). It can be seen from Figure 1a that the particle number concentration during the α-pinene photooxidation first increases and then decreases with the increase of either [NO] or [NO_2], indicating that the α-pinene-derived SOA formation is nonlinearly affected by the increase of [NO] or [NO_2]. Similarly, the increase of [NO_2] also shows a nonlinear effect on the Δ^3-carene-derived SOA formation (Figure 1c). However, the increase of [NO] shows a linear effect on the Δ^3-carene-derived SOA formation (Figure 1d).

With [NO_2] at ~50 ppb, the maximum particle number concentrations of α-pinene and Δ^3-carene are 4.9×10^4 and 4.2×10^4 particles/cm^3 (Figure 1a,1c), respectively. Increasing the NO_2 concentration to ~400 ppb, the maximum particle number concentrations of α-pinene and Δ^3-carene are 1.1×10^4 and 1.6×10^4 particles/cm^3, respectively, showing a decrease by 78 and 62% compared with the low [NO_2] condition (~50 ppb). This indicates that the suppression effect of NO_2 on the particle number concentration of the α-pinene photooxidation is more pronounced than that of the Δ^3-carene photooxidation. In contrast, with the increase of [NO] from ~50 to 400 ppb, the maximum particle number concentration of α-pinene and Δ^3-carene exhibits a decrease by 80 and 100% (Figure 1b,d), respectively, implying that the suppression effect of NO on the particle number concentration of the α-pinene photooxidation is less pronounced than that of the Δ^3-carene

https://doi.org/10.1021/acsearthspacechem.4c00159
ACS Earth Space Chem. 2024, 8, 1668−1679

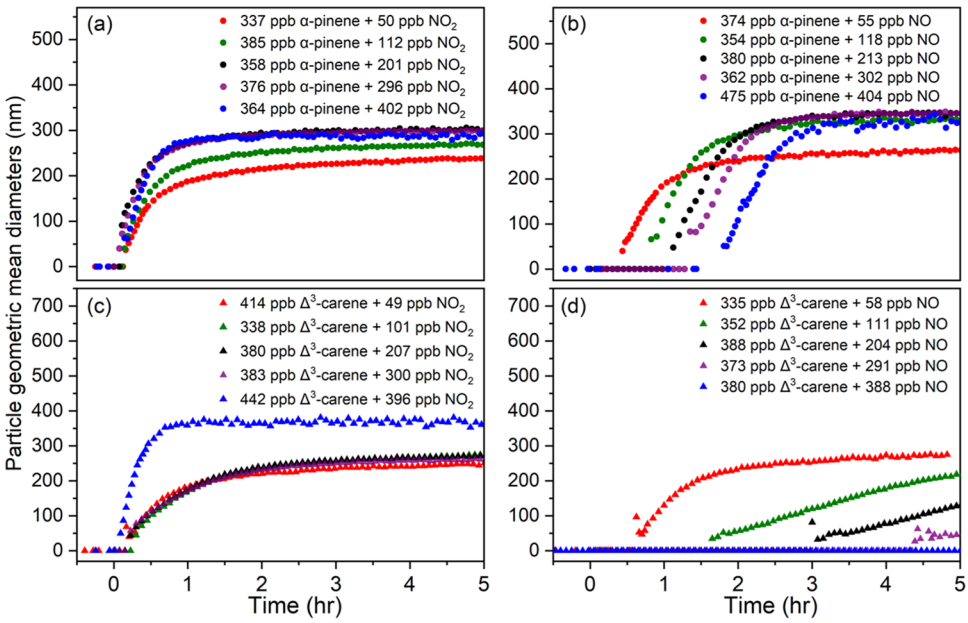

Figure 2. Size evolution of SOA produced in the photooxidation of α-pinene (a, b) and Δ^3-carene (c, d) under different NO and NO_2 concentrations. (d) All of the sizes of Δ^3-carene SOA are close to 280 nm except for the condition of [NO] = 388 ppb.

photooxidation. In particular, at the 380 ppb Δ^3-carene +388 ppb NO condition, no particles are observed. The particles are observable until the [NO] is tuned to 291 ppb.

Figure 2 illustrates the size evolution of SOA. As shown in Figure 2a, with raising [NO_2], the particle geometric mean diameter gradually increases and stabilizes when [NO_2] is 201 ppb. The particle geometric mean diameter in the 364 ppb α-pinene +402 ppb NO_2 condition is larger than that in the 377 ppb α-pinene +50 ppb NO_2 condition, indicating that the higher NO_2 concentration could promote the particle growth to a larger size. Similarly, the higher NO concentration also could enlarge the SOA size for the α-pinene photooxidation (Figure 2b). Although the α-pinene concentration of 475 ppb is slightly higher than other conditions, the effect on particle size is not obvious. The promotion effect of higher [NO_2] on the particle growth is also found in the photooxidation of Δ^3-carene (Figure 2c). When the [NO_2] increases from 49 to 396 ppb, the particle geometric mean diameter first remains almost unchanged and then shows an obvious increase. Such promotion effect may be attributed to the "rate effect" (SOA yield is higher with a faster oxidation rate).[23] With the increase of [NO_2], the oxidation rate of reactants increases significantly, which leads to a rapid rise in the concentration of semivolatiles and thereby favors the particle growth.[23] When the [NO_2] increases by approximately 350 ppb, the maximum size of SOA produced in the α-pinene photooxidation increases by around 50 nm (Figure 2a), whereas the maximum size of SOA produced in the Δ^3-carene photooxidation increases by approximately 120 nm (Figure 2c). This indicates that the NO_2 promotion effect on the SOA size growth of the α-pinene photooxidation is less pronounced than that of Δ^3-carene. It should be noted that under close [NO_2] conditions (~50 and ~400 ppb), the [Δ^3-carene] is slightly higher than the [α-pinene], which may influence the NO_2 promotion effect on the SOA size growth of the Δ^3-carene system. The higher concentrations of VOC precursor likely enhance the concentrations of RO_2 that consume NO_2 more quickly via the R(CO)OO + NO_2 → R(CO)OONO_2 reactions, allowing for the RO_2 + RO_2 or RO_2 + HO_2 termination reactions to enhance the growth of SOA. When the [NO] increases by about 350 ppb, the size of α-pinene SOA increases by around 70 nm (Figure 2b). While the [NO] increases by about 230 ppb (Figure 2d), the size of the Δ^3-carene SOA is almost unchanged (the maximum size of Δ^3-carene SOA is close to 280 nm). In addition, Figures S2 and S3 show that the appearance time of particles for α-pinene and Δ_3-carene system becomes later with the increase of [NO]. As shown in Figures S2c,d and S3c,d, the time profile of particle number concentration generally coincides with that of the NO-to-NO_2 conversion and the accumulation of O_3, implying that the accumulated O_3 might induce the conversion of VOC precursor into SOA. As shown in Figure 2, the conversion period for 404 ppb NO in the α-pinene system is even shorter than that of 204 ppb NO in the Δ^3-carene system, implying that NO has a more pronounced effect on the α-pinene and Δ^3-carene photooxidation than NO_2, which will be rationalized later (vide infra).

Figures S2 and S3 representatively show the [NO], [NO_2], [O_3], [α-pinene], [Δ^3-carene], and particle number concentrations, respectively. In the two systems, particles are detected when ozone begins to accumulate obviously. Meanwhile, significant amounts of monoterpenes remained; the particle number/size starts to grow when NO is depleted. It can be speculated that ozonolysis might play a key role in the α-pinene/Δ^3-carene + NO/NO_2 photooxidation reactions. For Figure 1a–c, the increase of particle number concentration with increasing [NO_x] may be due to the increase in [NO_x] leading to an increase in [O_3], thereby promoting particle generation; the decrease of particle number concentration with increasing [NO_x] may be due to the consumption of RO_2 by enhanced [NO_x]. In addition, NO_x promotes the OH production via the O_3 photolysis and the NO + HO_2 → NO_2 + OH reaction. However, the very high concentrations of NO_x might sink OH via the NO_2 + OH (+M) → HNO_3 (+M) reaction.

https://doi.org/10.1021/acsearthspacechem.4c00159
ACS Earth Space Chem. 2024, 8, 1668–1679

3.2. Effects of NO_x on the Chemical Components.

3.2.1. Mass Spectral Distribution. Figures S4−S7 show the mass spectra of products generated from the α-pinene and Δ^3-carene photooxidation, in which the main spectral features are consistent with previous studies.[17,20,33−35] The peak intensities were normalized relative to the highest peak. On the basis of the high-resolution characteristics of the Orbitrap Fusion Lumos Tribrid mass spectra, the molecular formulas of the ion peaks could be analyzed. In the present discussion, mass spectral analyses were mainly focused on the peaks with relative intensities larger than 1%. The molecular formulas and possible names of products identified in previous studies[17,20,33,34,36] are listed in Tables S1 and S2, respectively. Here, the compound containing less than 10 carbon atoms is referred to as a "monomer" and that with 11−20 carbon atoms is referred to as a "dimer."

For the α-pinene system, most components of SOA are observed in the low [NO_2] condition (Figure S4a) and the dimers (m/z > 250) are barely detected under the high [NO_2] and low/high [NO] conditions (Figures S4b−4e and S5). As shown in Figures S6 and S7, for the Δ^3-carene system, with the increase in [NO_2] and [NO], no significant changes are found in the overall mass spectra, especially in the m/z < 250 region (the monomers). These mass spectral results indicate that the changes of [NO_2] and [NO] exhibit a more pronounced effect on the compositions of the α-pinene-derived products than those of the Δ^3-carene-derived products. Here, the distribution of the mass spectrum in the two systems is analyzed by combining the time evolution of reactants and particles (Figures S2 and S3). In the VOC + NO_2 photooxidation, O_3 is formed from the photolysis of NO_2. The moment when O_3 starts to accumulate is about the 10th minute. Meanwhile, the ozonolysis of the higher concentration of VOC could produce more RO_2 intermediates, and dimers would be easily generated through the RO_2 + RO_2 reaction. Upon increasing [NO_2], the moment when O_3 begins to accumulate is basically unchanged (the 10th minute), but higher concentrations of NO_x consume more RO_2, reducing dimer products. In the photooxidation of VOC + NO, NO is first converted into NO_2, and then the photolysis of NO_2 produces O_3. The moment when O_3 begins to accumulate is basically consistent with the time of complete NO-to-NO_2 conversion. The increase of [NO] causes a gradual delay for the accumulation time of O_3. In the photooxidation of VOC + NO_2, the amount of VOC involved in the ozonolysis is lower, resulting in a lower particle number concentration. Note that the ozonolysis rate of Δ^3-carene is slower ($k_{\alpha\text{-pinene}}$ = 8.7 × 10^{-17} cm^3 $molecule^{-1}$ s^{-1}, $k_{\Delta^3\text{-carene}}$ = 4.4 × 10^{-17} cm^3 $molecule^{-1}$ s^{-1}).[37] The reaction of RO_2 + RO_2 may be easier to proceed in the Δ^3-carene system. Therefore, the increase in [NO_2] or [NO] shows a weak effect on the composition of Δ^3-carene products. The peak numbers of m/z < 170 in the Δ^3-carene system (Figures S6 and S7) are much more than those in the α-pinene system (Figures S4 and S5), which may be ascribed to the instability of Δ^3-carene's three-membered ring. Namely, the intermediates with three-membered ring might readily undergo a ring-opening reaction and produce substances with smaller mass numbers, resulting in the enhanced fragmentation chemistry.

Besides the aforementioned carbohydrate products, a few nitrogen-containing compounds are also observed via the analysis of mass spectra. In this study, the N-containing species might be primarily produced from the RO_2 + NO or acyl RO_2 + NO_2 reactions. NO_3 is a kind of tipicaly oxidant in the atmospheric system containing NO_x. However, NO_3 is readily to photolysis under photooxidation conditions, an accurate description of the reaction of NO_3 with VOC is thus challenging and is not detailed in this phooxidation study. Under the condition that NO_2 is the main component of NO_x, particles generated before NO is depleted. It is speculated that the N-containing species may be originated from the two pathways of acyl RO_2 + NO_2 and RO_2 + NO. However, under the condition that NO is the main component of NO_x, particles generated after NO is depleted, and it is speculated that the N-containing species may be mainly originated from the acyl RO_2 + NO_2 pathway. In the α-pinene system, $C_{22}H_{37}O_3N$ is obtained under low [NO_2] condition and $C_{18}H_{31}O_5N_2$ and $C_{19}H_{35}O_5N_2$ are obtained under low [NO] condition. In the Δ^3-carene system, $C_{10}H_{15}O_8N$ and $C_{10}H_{17}O_8N$ are obtained under high [NO_2] condition, $C_7H_9O_9N$ and $C_{18}H_{40}O_7N_2$ are obtained under low [NO] condition, and $C_9H_{16}O_{13}N$, $C_{10}H_{16}O_{10}N_2$, $C_{10}H_{17}O_{12}N_3$, $C_{16}H_{36}O_7N_2$, $C_{18}H_{40}O_7N_2$, and $C_{23}H_{33}O_5N$ are obtained under high [NO] condition containing more than 20 carbon atoms (>C_{20}) products mentioned in this study could be one of the isomers, which may be formed from dimers and fragment intermediates. Thus, the photooxidation of Δ^3-carene produces more nitrogen-containing compounds than that of α-pinene. It could be speculated that semivolatiles (formed from the RO_2 + NO reaction) are more likely produced during the Δ^3-carene oxidation and condense on the particle surfaces. The increase of [NO] consumes more RO_2 to enhance the formation of high-volatile organic nitrates that suppress the SOA nucleation, which is in accord with previous results.[11,25] As observed in Figure 1, the NO inhibition effect on the Δ^3-carene photooxidation is more pronounced than that on the α-pinene photooxidation. This observation further supports the hypothesis that the photooxidation of Δ^3-carene with NO is more likely to form high-volatile organic nitrates than that of α-pinene.

3.2.2. Effects of NO_x on the H/C and O/C Ratios. A visual picture of the H/C and O/C ratios of SOA components could be obtained from the Van Krevelen diagram,[36] in which a higher H/C value stands for a lower degree of molecular unsaturation and a higher O/C value denotes a higher degree of oxidation. Accordingly, such Van Krevelen diagrams for α-pinene and Δ^3-carene at the lowest/highest [NO_2] and the lowest/highest [NO] are plotted in Figures 3 and 4, respectively. The separate Van Krevelen diagrams for α-pinene and Δ^3-carene at all of the [NO_2] and [NO] concentrations are summarized in Figures S8 and S9, respectively. The mean values of the H/C and O/C ratios are given in Table S3. Note that the O/C value in the real environment is larger than that in the laboratory condition, owing to the sufficient time for aging in the atmospheric condition.[38]

The mean H/C values in the Δ^3-carene system are slightly lower than those in the α-pinene system (Table S3), indicative of a higher degree of molecular unsaturation of Δ^3-carene-derived products. The mean O/C values in the Δ^3-carene system are close to those in the α-pinene system. The number of higher O/C products in the Δ^3-carene system is larger than those in the α-pinene system, indicating that Δ^3-carene could be more favorable for the formation of highly oxidized products. Increasing the O/C value lowers the alcohol content but raises the carboxylic acid content.[39,40] This means that the product is less volatile and has a higher potential for separation in the particle phase. However, the overall particle number

https://doi.org/10.1021/acsearthspacechem.4c00159
ACS Earth Space Chem. 2024, 8, 1668−1679

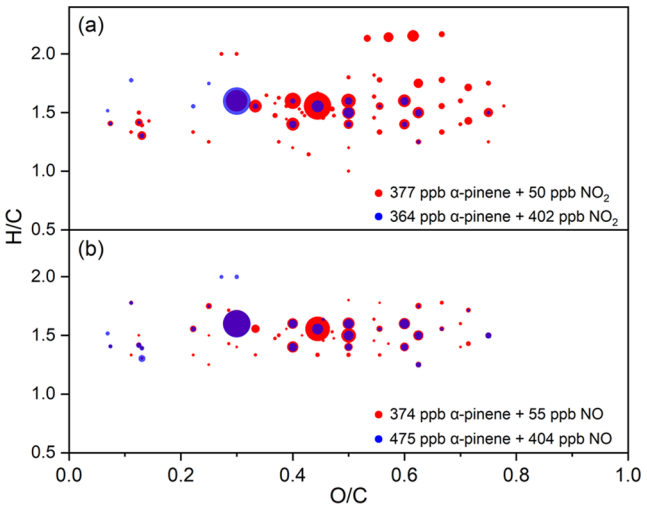

Figure 3. Van Krevelen diagram of H/C vs O/C of SOA components in the α-pinene photooxidation at the lowest/highest [NO_2] (a) and the lowest/highest [NO] (b).

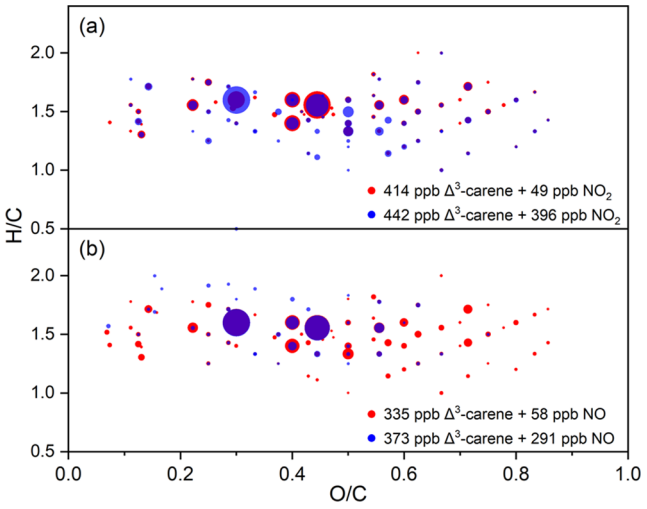

Figure 4. Van Krevelen diagram of H/C vs O/C of SOA components in the Δ^3-carene photooxidation at the lowest/highest [NO_2] (a) and the lowest/highest [NO] (b).

concentrations and particle sizes for α-pinene are larger than those for Δ^3-carene. Therefore, the high O/C value of SOA stemmed from Δ^3-carene system may originate from other reasons. The distribution of O/C vs n_C of the two systems is shown in Figure S10. The products formed from Δ^3-carene with the higher O/C were mainly distributed in areas with low n_C values. Thus, the larger degree of fragmentation (smaller C) might be the dominant reason for the higher O/C in the Δ^3-carene-derived aerosols. As far as we know, limited research has been conducted on the comparison of the autoxidation capacity of α-pinene and Δ^3-carene. The findings in Section 3.3 of this study support the notion that the intermediates of Δ^3-carene exhibit a stronger autoxidation capacity based on theoretical calculations (vide infra). Thus, the higher O/C in the Δ^3-carene SOA might be due to the larger degree of fragmentation and the stronger autoxidation capacity of Δ^3-carene.

As listed in Table S3, as the concentration of NO_2 or NO increases linearly, the O/C value changes in a nonlinear trend. Upon increasing [NO_2], the O/C value of α-pinene-derived SOA decreases from 0.46 to 0.37 and passes through a maximum (0.49 at [NO_2] ~296 ppb). It implies that the oxidation degree of products under high [NO_2] condition is lowered and thus makes the SOA nucleation more difficult, which supports the decrease of particle number concentration upon increasing [NO_2] (Figure 1a). In contrast, the increase of [NO_2] or [NO] makes an insignificant change in the O/C value for the Δ^3-carene system. It is worth noting that ΔM in the Δ^3-carene system increases obviously under high [NO_2] condition (Table 1). This indicates that the increase in the mass of a single particle (Figure 2c) might buffer the decrease in the number of particles (Figure 1c), ultimately resulting in an enhancement of the SOA yield.

3.2.3. Effects of NO_x on the Volatility of SOA Components. Figures 5 and 6 show the oxidation state of carbon (OS_C, OS_C $= 2 \times O/C - H/C$)[41] as a function of carbon number (n_C) of SOA components in the α-pinene and Δ^3-carene photooxidation, respectively. The shape area represents the normalized intensity of the mass spectral peak, and the color represents the $\log_{10} C^*$ (C^*: mass saturation concentration of the molecule).[42] $\log_{10} C^*_i$ is given by eq 1

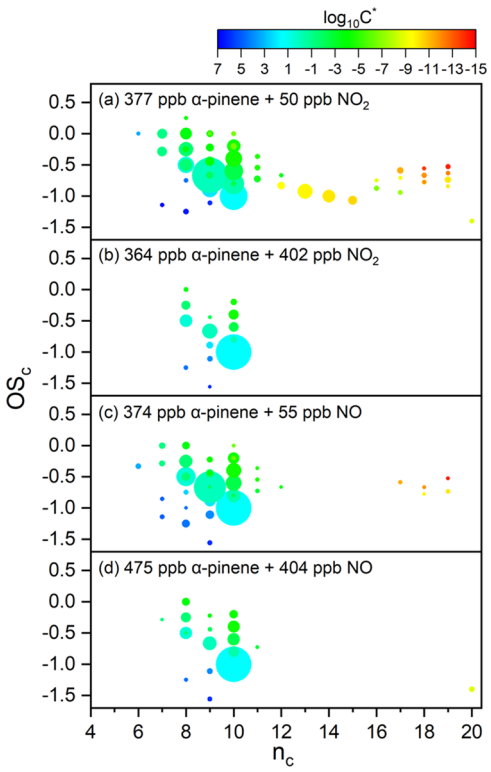

Figure 5. OS_C as a function of n_C in the α-pinene photooxidation under different NO_2 (a, b) and NO (c, d) concentrations. The area of the shape represents the normalized intensity of the mass spectral peak. The color represents the $\log_{10} C^*$ (C^* is the mass saturation concentration of the molecule).

$$\log_{10} C_i^* = (n_C^0 - n_C^i)b_C - n_O^i b_O - 2\frac{n_C^i n_O^i}{n_C^i + n_O^i} b_{CO} \quad (1)$$

where n_C^0 stands for the carbon number of alkane (1 μg m^{-3}), b_C for the C−C interaction, b_O for the O−O interaction, b_{CO} for the C−O nonideality, n^i_C for the number of C atoms of a given compound, and n^i_O for the number of O atoms of a given compound.

https://doi.org/10.1021/acsearthspacechem.4c00159
ACS Earth Space Chem. 2024, 8, 1668−1679

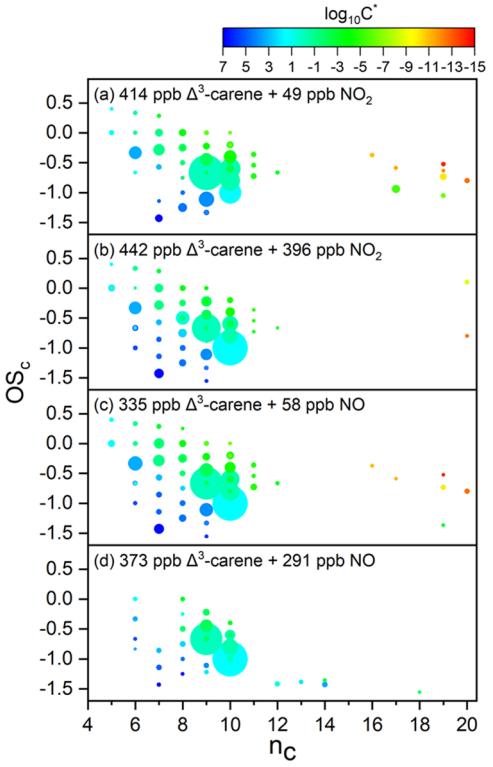

Figure 6. OS_C as a function of n_C in the Δ^3-carene photooxidation under different NO_2 (a, b) and NO (c, d) concentrations. The area of the shape represents the normalized intensity of the mass spectral peak. The color represents the $\log_{10} C^*$ (C^* is the mass saturation concentration of the molecule).

In general, organic products can be classified into five grades: (1) $C^* < 3 \times 10^{-4}$ $\mu g/m^3$, extremely low-volatile organic compound (ELVOC); (2) $3 \times 10^{-4} < C^* < 0.3$ $\mu g/m^3$, low-volatility organic compound (LVOC); (3) $0.3 < C^* < 300$ $\mu g/m^3$, semivolatile organic compound (SVOC); (4) $300 < C^* < 3 \times 10^6$ $\mu g/m^3$, intermediate-volatility organic compound (IVOC); and (5) $C^* > 3 \times 10^6$ $\mu g/m^3$, VOC.[43] Lower volatile species readily reach their supersaturated concentration and thus are favorable for the SOA nucleation. Previous studies on the α-pinene ozonolysis have demonstrated that the $C_{10}H_{14}O_{6,8,10}$ monomers contribute to the particle growth and the $C_{20}H_{30}O_{8-16}$ dimers are the primary compounds involved in the particle nucleation.[44,45] The field measurement of SOA generated by the interactions between anthropogenic pollutants and BVOCs in cities near tropical rainforests indicates that ELVOC plays a vital role in the early stage of SOA generation and SVOC donates to the rapid growth of particles.[46] As shown in Figures 5 and 6, the number of products with high OS_C values in α-pinene and Δ^3-carene systems gradually decreases with the increase of n_C, implying that only partial oxidation reactions of VOC precursor could produce dimer products with high n_C. Thus, the radical initiation, propagation, and termination reaction processes could be engaged in the α-pinene and Δ^3-carene oxidations.[1,41] These processes also serve as the foundation for the RO_2 autoxidation in the highly oxidized organic molecule (HOM) generation. Moreover, the volatility of molecules with the same n_C decreases as the OS_C value increases, and most of the dimers can be classified as ELVOCs.

For the α-pinene system (Figure 5), the number and abundance of C_{7-10} HOM monomers remarkably decrease with increasing $[NO_2]$ or [NO], with the absence of HOM dimers at high $[NO_x]$. These suppression effects of high $[NO_x]$ make difficulties for the SOA formation, which are consistent with the aforementioned O/C results. That is, under high $[NO_x]$ conditions, the creation of highly oxidized and low-volatile products is hindered, which reduces the particle number concentration, which is consistent with previous studies.[44,47] For the Δ^3-carene system (Figure 6), with the increase of $[NO_2]$, there are no significant changes in the number and abundance of the monomers but with some increase of the types (i.e., the C_{6-9} species), whereas those of dimers decrease significantly. It can be inferred from the above analyses that for α-pinene and Δ^3-carene, the increase of $[NO_2]$ or [NO] has a different effect on the monomers but a similar effect on the dimers.

There are a few assumptions that we would put forward: (1) Since the SOA particles were collected with methanol for mass spectral measurement, some compounds that are not soluble in methanol may elude the detection by the Orbitrap mass spectrometer. (2) Since the $\log_{10} C^*$ calculation for the volatility is based on an empirical formula and does not take into account the exact structure of the molecule, the estimated volatility of the molecule may have some bias. The monomer products might possess unique molecular structures with lower volatility. (3) There may be unidentified mechanisms by which the low-mass products with higher volatility also contribute to the SOA formation. (4) Considering that the stability of Δ^3-carene's three-membered ring is worse than that of α-pinene's four-membered ring and the photolysis of NO_2 can generate $O(^3P)$ to produce O_3 more directly than that of NO ($NO_2 \rightarrow O(^3P) + NO$; $NO \rightarrow NO_2 \rightarrow O(^3P)$; $O(^3P) + O_2 \rightarrow O_3$), the "rate effect" in the SOA formation with high $[NO_2]$ may be more obvious for Δ^3-carene than for α-pinene. The highly concentrated semivolatiles formed in a short time are either physically or chemically absorbed by particles, which reduces the particle number concentration but improves the particle size (as depicted in Figures 1c and 2c).

3.3. Photooxidation Mechanisms of α-Pinene and Δ^3-Carene. The OH concentration was difficult to be measured in the present experiments and then its role in the photooxidation processes could not be definitively identified. In the previous study,[24] based on the O_3 concentration and the decay rate of isoprene in the VOCs + NO_x photooxidation, O_3 was found to be crucial for the SOA formation. Thus, O_3 is also assumed to be the dominant oxidant in this study. Considering that O_3 is one of the most important oxidants in the VOC photooxidation by NO_x,[21,24] we mainly discuss the autoxidation capabilities of α-pinene and Δ^3-carene. Figure S11 shows the possible pathways of the α-pinene and Δ^3-carene ozonolysis. Products and intermediates derived from α-pinene and Δ^3-carene are prefixed with α- and Δ-, respectively. The α-pinene and Δ^3-carene ozonolysis can produce RO_2 for the subsequent autoxidation processes. The unimolecular H-shift pathways of cyclobutyl ring-RO_2 (CB-RO_2)[48] and cyclopropyl ring-RO_2 (CP-RO_2) are found to be very slow and thus not favorable for subsequent autoxidation. The isomerization pathways for CP-RO_2 are shown in Figure S12, with the smallest barrier of 21.1 kcal/mol. Previous study[49] indicated that α-vinoxy readily undergoes a ring-opening reaction, which triggers rapid autoxidation and forms a peroxy radical α-O8-RO_2 containing eight oxygen atoms. Therefore, the ring-opening reaction of vinoxy might be the key process in the subsequent autoxidation of α-pinene and Δ^3-carene. The

https://doi.org/10.1021/acsearthspacechem.4c00159
ACS Earth Space Chem. 2024, 8, 1668−1679

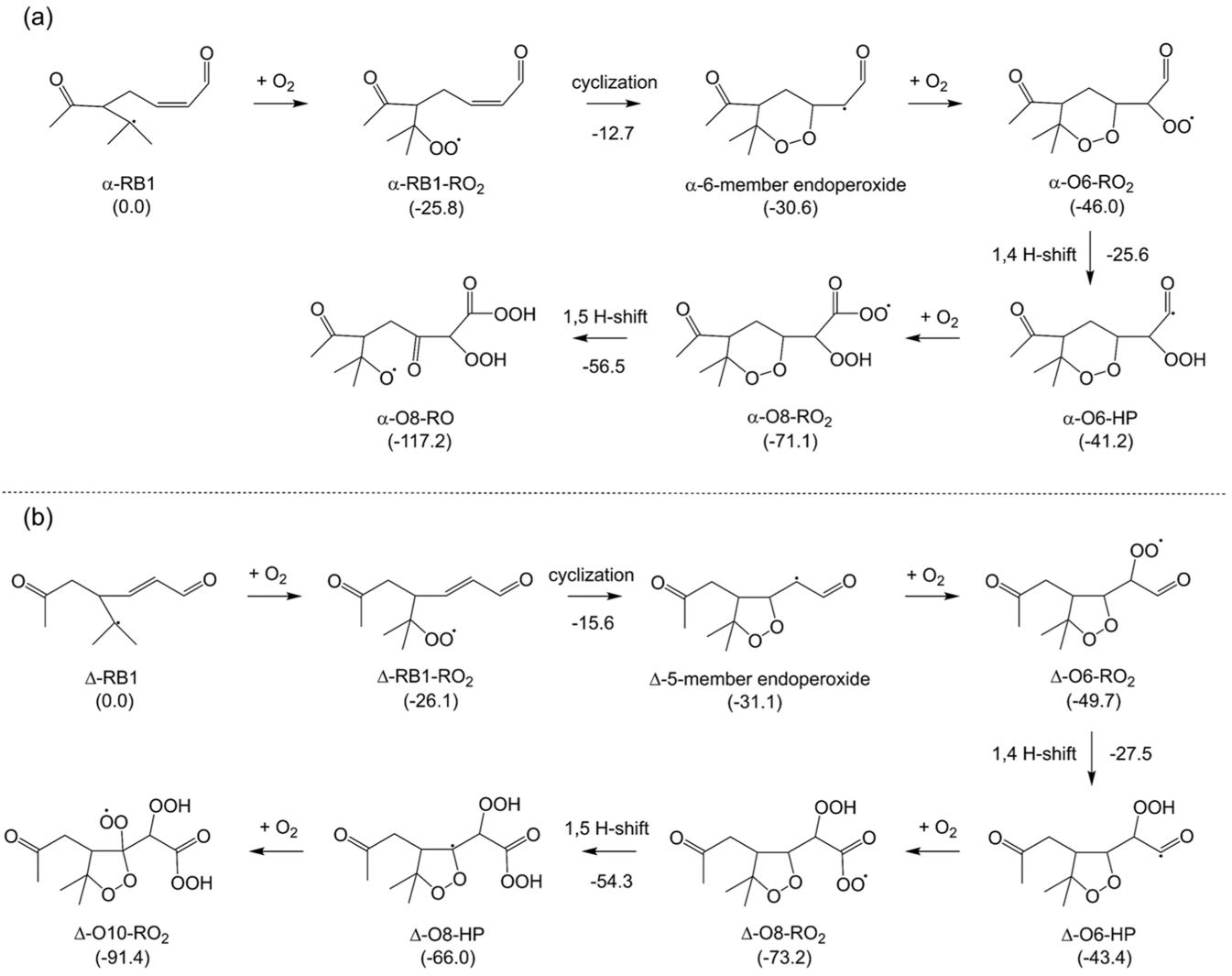

Figure 7. Autoxidation pathways of α-RB1 (a) and Δ-RB1 (b) calculated at the ωB97XD/def2-TZVP level of theory. Relative energies are given in kcal/mol. The values in brackets and below the arrows are the relative energies of intermediates and transition states, respectively.

energy barrier for the ring-opening reaction of α-vinoxy[49] is predicted to be 14.6 kcal/mol, while those of Δ-vinoxy are calculated to be much smaller (Δ-RB1, 8.0 kcal/mol; Δ-RB2, 8.6 kcal/mol) (Figure S13). It could be rationalized that the bond tension of Δ^3-carene's three-membered ring is larger than that of α-pinene's four-membered ring, which makes the Δ-vinoxy more readily to undergo the first step of autoxidation. Even though the α-pinene-derived Criegee intermediate 2 (α-CI2) has the structural characteristics for a direct ring-opening reaction, the ring-opened products are still difficult to be formed due to the high energy barrier.[49] The Δ^3-carene-derived CIs (Δ-CI1 and Δ-CI2) cannot be directly isomerized to the ring-opened structures due to the distribution of radical site.

Figure 7 shows the energetic information on favorable autoxidation steps of α-RB1 and Δ-RB1. As shown in Figure 7a, after three steps of α-RB1 oxidation with O_2, α-O8-RO_2 could further undergo isomerization via 1,5 H-shift to form the ring-opened alkoxy radical α-O8-RO, with an exothermic value of 46.1 kcal/mol and a barrier of 14.6 kcal/mol. Our calculations indicate that it is very difficult to obtain a stable carbon-centered radical via the isomerization of α-O8-RO_2. Therefore, α-RB1 could undergo three steps of autoxidation. After the RO_2 + NO and RO_2 + HO_2 terminal reactions, the *O*/*C* ratio of HOMs is in the 0.6−0.9 region.

As illustrated in Figure 7b, the addition of O_2 onto Δ-RB1 forms Δ-RB1-RO_2 is exothermic by 26.1 kcal/mol. Δ-RB1-RO_2 undergoes cyclization to form Δ-5-member endoperoxide with an exothermic value of 5.0 kcal/mol and a barrier value of 10.5 kcal/mol, which energetics is similar to that of the α-RB1-RO_2 → α-6-member endoperoxide cyclization of the α-pinene system (exothermic value, 4.8 kcal/mol; energy barrier, 13.1 kcal/mol). This indicates that Δ-RB1 could also undergo a second step of oxidation with O_2. After the third step of Δ-RB1 oxidation with O_2, Δ-O8-RO_2 could undergo further isomerization via 1,5 H-shift to form Δ-O8-HP, which process is slightly endothermic by 7.2 kcal/mol and overcomes a barrier of 18.9 kcal/mol. The exothermic value for the subsequent reaction of Δ-O8-HP with O_2 to form Δ-O10-RO_2 is 25.4 kcal/mol. The energy barrier for 1,4 H-shift on the ring and outside the ring of Δ-O10-RO_2 is as large as 26.4 and 28.5 kcal/mol, respectively, making it difficult for further autoxidation. Accordingly, Δ-RB1 could undergo four steps of autoxidation, and the O/C ratio of HOMs is in the 0.6−1.1 region. Thus, Δ^3-carene is more likely to generate the products with a higher degree of oxidation compared with α-pinene,

https://doi.org/10.1021/acsearthspacechem.4c00159
ACS Earth Space Chem. 2024, 8, 1668−1679

supporting the experimental results as shown in Figures 3 and 4. Note that it might be challenging to measure the mass spectra of some highly oxidized products with low yields.

Under atmospheric conditions, the radical chain reaction is generally ended by RO_2 + NO_x and RO_2 + HO_2. For α-pinene and Δ^3-carene, the terminal products of the first-generation autoxidation intermediate $C_{10}H_{15}O_4$ (α-RB1-RO_2 and Δ-RB1-RO_2) and the second-generation autoxidation intermediate $C_{10}H_{15}O_6$ (α-O6-RO_2 and Δ-O6-RO_2) with HO_2 is $C_{10}H_{16}O_4$ and $C_{10}H_{16}O_6$, respectively, which corresponds to the peak at 199 and 231 in the negative ion mass spectra of Figures S4–S7. However, the terminal products of these intermediates with NO are rarely observed, which could be rationalized that the volatility of nitrate products generated from the RO_2 + NO reaction is higher than that of hydroperoxide products generated from the RO_2 + HO_2 reaction. The terminal products of the third-generation autoxidation intermediates (α-O8-RO_2 and Δ-O8-RO_2) and fourth-generation autoxidation intermediate (Δ-O10-RO_2) are barely detectable.

4. CONCLUSIONS AND ATMOSPHERIC IMPLICATIONS

The photooxidation experiments of isomeric VOCs of α-pinene and Δ^3-carene in the presence of a specific NO_x component (NO_2 and NO) were conducted under different concentrations. Multifaceted impacts of NO_x on the SOA formation are found and discussed at the molecular level. The results indicate that the increased NO_x concentrations suppress the particle number concentrations for both α-pinene and Δ^3-carene, which might be due to the decrease of high-oxygen-content products and low-volatile dimers. On the other hand, the increased NO_x concentrations enhance the growth of particle size (except for the photooxidation of Δ^3-carene with NO), which might buffer the suppression effect of NO_x.

The highly oxidized and low-volatile products are difficult to be formed at high [NO_x], which consequently suppresses the SOA nucleation and decreases the SOA yield. This finding agrees with previous studies,[11,25,47] implying that RO_2 is important in SOA formation. The reaction of Δ^3-carene with oxidants generated by direct NO_2 photolysis might exhibit a noticeable rate effect under high [NO_2] condition. This effect enhances the particle growth and buffers the reduction of particle number concentration, which improves the particle mass concentration. Consequently, higher [NO_2] (101–396 ppb) promotes the SOA yield for the Δ^3-carene photooxidation. On the other hand, different structures of α-pinene and Δ^3-carene show a distinct influence on the SOA formation. The number of products with higher O/C in the Δ^3-carene system is larger than that in the α-pinene system.

Quantum chemical calculations of autoxidation processes indicate that the ring-opening reaction of Δ-vinoxy derived from Δ^3-carene is more favorable than that of α-vinoxy derived from α-pinene. Δ-Vinoxy could undergo four steps of autoxidation to form Δ-O10-RO_2, whereas α-vinoxy only undergoes three steps of autoxidation to form α-O8-RO_2. The terminal products of Δ^3-carene have a higher oxygen content than those of α-pinene, which may partially account for the higher O/C value for Δ^3-carene. The different effects of NO_x on the α-pinene and Δ^3-carene photooxidation could be rationalized that the bond tension of Δ^3-carene's three-membered ring is larger than that of α-pinene's four-membered ring. The present findings advance our mechanical understanding of the interactions between NO_x and isomeric monoterpenes and stimulate further experimental and theoretical studies on a large variety of isomeric VOCs toward the improvement of SOA models.

■ ASSOCIATED CONTENT

Supporting Information

The Supporting Information is available free of charge at https://pubs.acs.org/doi/10.1021/acsearthspacechem.4c00159.

SOA mass spectra of first and second extractions (Figure S1); [NO], [NO_2], [O_3], [α-pinene], [Δ^3-carene], and particle number concentrations (Figures S2 and S3); mass spectra (Figures S4–S7); Van Krevelen diagram under different NO_x (Figures S8 and S9), distribution of O/C vs n_C (Figure S10); ozonolysis reactions (Figure S11); H-shift isomerization pathways for CP-RO_2 (Figure S12); ring-opening isomerization pathways for α-vinoxy and Δ-vinoxy (Figure S13); molecular weights, formulas, and names of products (Tables S1 and S2); mean values of H/C and O/C (Table S3) (PDF)

■ AUTHOR INFORMATION

Corresponding Authors

Gang Li − *State Key Laboratory of Molecular Reaction Dynamics, Dalian Institute of Chemical Physics, Chinese Academy of Sciences, Dalian 116023, China; University of Chinese Academy of Sciences, Beijing 100049, China;* orcid.org/0000-0001-5984-111X; Email: gli@dicp.ac.cn

Ling Jiang − *State Key Laboratory of Molecular Reaction Dynamics, Dalian Institute of Chemical Physics, Chinese Academy of Sciences, Dalian 116023, China; University of Chinese Academy of Sciences, Beijing 100049, China; Hefei National Laboratory, Hefei 230088, China;* orcid.org/0000-0002-8485-8893; Email: ljiang@dicp.ac.cn

Authors

Zhaoyan Zhang − *State Key Laboratory of Molecular Reaction Dynamics, Dalian Institute of Chemical Physics, Chinese Academy of Sciences, Dalian 116023, China; University of Chinese Academy of Sciences, Beijing 100049, China*

Xiangyu Zang − *State Key Laboratory of Molecular Reaction Dynamics, Dalian Institute of Chemical Physics, Chinese Academy of Sciences, Dalian 116023, China; Technology Center for China Tobacco Henan Industrial Limited Company, Zhengzhou 450016, China*

Yingqi Zhao − *State Key Laboratory of Molecular Reaction Dynamics, Dalian Institute of Chemical Physics, Chinese Academy of Sciences, Dalian 116023, China; University of Chinese Academy of Sciences, Beijing 100049, China*

Ya Zhao − *State Key Laboratory of Molecular Reaction Dynamics, Dalian Institute of Chemical Physics, Chinese Academy of Sciences, Dalian 116023, China*

Hua Xie − *State Key Laboratory of Molecular Reaction Dynamics, Dalian Institute of Chemical Physics, Chinese Academy of Sciences, Dalian 116023, China; University of Chinese Academy of Sciences, Beijing 100049, China;* orcid.org/0000-0003-2091-6457

Xueming Yang − *State Key Laboratory of Molecular Reaction Dynamics, Dalian Institute of Chemical Physics, Chinese Academy of Sciences, Dalian 116023, China; University of Chinese Academy of Sciences, Beijing 100049, China; Hefei*

National Laboratory, Hefei 230088, China; Department of Chemistry and Guangdong Provincial Key Laboratory of Catalytic Chemistry, Southern University of Science and Technology, Shenzhen 518055, China; orcid.org/0000-0001-6684-9187

Complete contact information is available at: https://pubs.acs.org/10.1021/acsearthspacechem.4c00159

Author Contributions

#Z.Z. and X.Z. contributed equally to this work.

Notes

The authors declare no competing financial interest.

■ ACKNOWLEDGMENTS

The authors gratefully acknowledge the Dalian Coherent Light Source (DCLS) for support and assistance. This work was supported by the National Natural Science Foundation of China (Nos. 22125303, 92361302, 92061203, 22373102, 22103082, and 22288201), the National Key Research and Development Program of China (No. 2021YFA1400501), the Innovation Program for Quantum Science and Technology (No. 2021ZD0303304), the Dalian Institute of Chemical Physics (No. DICP I202437), and the Chinese Academy of Sciences (No. GJJSTD20220001).

■ REFERENCES

(1) Hallquist, M.; Wenger, J. C.; Baltensperger, U.; Rudich, Y.; Simpson, D.; Claeys, M.; Dommen, J.; Donahue, N. M.; George, C.; Goldstein, A. H.; Hamilton, J. F.; Herrmann, H.; Hoffmann, T.; Iinuma, Y.; Jang, M.; Jenkin, M. E.; Jimenez, J. L.; Kiendler-Scharr, A.; Maenhaut, W.; McFiggans, G.; Mentel, T. F.; Monod, A.; Prevot, A. S. H.; Seinfeld, J. H.; Surratt, J. D.; Szmigielski, R.; Wildt, J. The formation, properties and impact of secondary organic aerosol: current and emerging issues. *Atmos. Chem. Phys.* **2009**, *9*, 5155−5236.

(2) Brauer, M.; Freedman, G.; Frostad, J.; van Donkelaar, A.; Martin, R. V.; Dentener, F.; van Dingenen, R.; Estep, K.; Amini, H.; Apte, J. S.; Balakrishnan, K.; Barregard, L.; Broday, D.; Feigin, V.; Ghosh, S.; Hopke, P. K.; Knibbs, L. D.; Kokubo, Y.; Liu, Y.; Ma, S.; Morawska, L.; Texcalac Sangrador, J. L.; Shaddick, G.; Anderson, H. R.; Vos, T.; Forouzanfar, M. H.; Burnett, R. T.; Cohen, A. Ambient air pollution exposure estimation for the global burden of disease 2013. *Environ. Sci. Technol.* **2016**, *50*, 79−88.

(3) Shiraiwa, M.; Ueda, K.; Pozzer, A.; Lammel, G.; Kampf, C. J.; Fushimi, A.; Enami, S.; Arangio, A. M.; Froehlich-Nowoisky, J.; Fujitani, Y.; Furuyama, A.; Lakey, P. S. J.; Lelieveld, J.; Lucas, K.; Morino, Y.; Poeschl, U.; Takaharna, S.; Takami, A.; Tong, H.; Weber, B.; Yoshino, A.; Sato, K. Aerosol health effects from molecular to global scales. *Environ. Sci. Technol.* **2017**, *51*, 13545−13567.

(4) Lewis, A. C. The changing face of urban air pollution. *Science* **2018**, *359*, 744−745.

(5) Sindelarova, K.; Granier, C.; Bouarar, I.; Guenther, A.; Tilmes, S.; Stavrakou, T.; Muller, J. F.; Kuhn, U.; Stefani, P.; Knorr, W. Global data set of biogenic VOC emissions calculated by the MEGAN model over the last 30 years. *Atmos. Chem. Phys.* **2014**, *14*, 9317−9341.

(6) Zhang, H.; Yee, L. D.; Lee, B. H.; Curtis, M. P.; Worton, D. R.; Isaacman-VanWertz, G.; Offenberg, J. H.; Lewandowski, M.; Kleindienst, T. E.; Beaver, M. R.; Holder, A. L.; Lonneman, W. A.; Docherty, K. S.; Jaoui, M.; Pye, H. O. T.; Hu, W.; Day, D. A.; Campuzano-Jost, P.; Jimenez, J. L.; Guo, H.; Weber, R. J.; de Gouw, J.; Koss, A. R.; Edgerton, E. S.; Brune, W.; Mohr, C.; Lopez-Hilfiker, F. D.; Lutz, A.; Kreisberg, N. M.; Spielman, S. R.; Hering, S. V.; Wilson, K. R.; Thornton, J. A.; Goldstein, A. H. Monoterpenes are the largest source of summertime organic aerosol in the southeastern United States. *Proc. Natl. Acad. Sci. U.S.A.* **2018**, *115*, 2038−2043.

(7) Goldstein, A. H.; Galbally, I. E. Known and unexplored organic constituents in the earth's atmosphere. *Environ. Sci. Technol.* **2007**, *41*, 1514−1521.

(8) Sakulyanontvittaya, T.; Duhl, T.; Wiedinmyer, C.; Helmig, D.; Matsunaga, S.; Potosnak, M.; Milford, J.; Guenther, A. Monoterpene and sesquiterpene emission estimates for the United States. *Environ. Sci. Technol.* **2008**, *42*, 1623−1629.

(9) Ng, N. L.; Kroll, J. H.; Keywood, M. D.; Bahreini, R.; Varutbangkul, V.; Flagan, R. C.; Seinfeld, J. H.; Lee, A.; Goldstein, A. H. Contribution of first- versus second-generation products to secondary organic aerosols formed in the oxidation of biogenic hydrocarbons. *Environ. Sci. Technol.* **2006**, *40*, 2283−2297.

(10) Hoyle, C. R.; Boy, M.; Donahue, N. M.; Fry, J. L.; Glasius, M.; Guenther, A.; Hallar, A. G.; Hartz, K. H.; Petters, M. D.; Petaja, T.; Rosenoern, T.; Sullivan, A. P. A review of the anthropogenic influence on biogenic secondary organic aerosol. *Atmos. Chem. Phys.* **2011**, *11*, 321−343.

(11) Presto, A. A.; Hartz, K. E. H.; Donahue, N. M. Secondary organic aerosol production from terpene ozonolysis. 2. Effect of NO_x concentration. *Environ. Sci. Technol.* **2005**, *39*, 7046−7054.

(12) Pathak, R. K.; Stanier, C. O.; Donahue, N. M.; Pandis, S. N.Ozonolysis of α-pinene at atmospherically relevant concentrations: temperature dependence of aerosol mass fractions (yields) *J. Geophys. Res.: Atmos.* 2007; Vol. *112* DOI: 10.1029/2006JD007436.

(13) Ehn, M.; Thornton, J. A.; Kleist, E.; Sipila, M.; Junninen, H.; Pullinen, I.; Springer, M.; Rubach, F.; Tillmann, R.; Lee, B.; Lopez-Hilfiker, F.; Andres, S.; Acir, I. H.; Rissanen, M.; Jokinen, T.; Schobesberger, S.; Kangasluoma, J.; Kontkanen, J.; Nieminen, T.; Kurten, T.; Nielsen, L. B.; Jorgensen, S.; Kjaergaard, H. G.; Canagaratna, M.; Dal Maso, M.; Berndt, T.; Petaja, T.; Wahner, A.; Kerminen, V.-M.; Kulmala, M.; Worsnop, D. R.; Wildt, J.; Mentel, T. F. A large source of low-volatility secondary organic aerosol. *Nature* **2014**, *506*, 476−479.

(14) Sarrafzadeh, M.; Wildt, J.; Pullinen, I.; Springer, M.; Kleist, E.; Tillmann, R.; Schmitt, S. H.; Wu, C.; Mentel, T. F.; Zhao, D.; Hastie, D. R.; Kiendler-Scharr, A. Impact of NO_x and OH on secondary organic aerosol formation from β-pinene photooxidation. *Atmos. Chem. Phys.* **2016**, *16*, 11237−11248.

(15) Bäck, J.; Aalto, J.; Henriksson, M.; Hakola, H.; He, Q.; Boy, M. Chemodiversity of a Scots pine stand and implications for terpene air concentrations. *Biogeosciences* **2012**, *9*, 689−702.

(16) Ma, Y.; Porter, R. A.; Chappell, D.; Russell, A. T.; Marston, G. Mechanisms for the formation of organic acids in the gas-phase ozonolysis of 3-carene. *Phys. Chem. Chem. Phys.* **2009**, *11*, 4184−4197.

(17) Glasius, M.; Lahaniati, M.; Calogirou, A.; Di Bella, D.; Jensen, N. R.; Hjorth, J.; Kotzias, D.; Larsen, B. R. Carboxylic acids in secondary aerosols from oxidation of cyclic monoterpenes by ozone. *Environ. Sci. Technol.* **2000**, *34*, 1001−1010.

(18) Roldin, P.; Liao, L.; Mogensen, D.; Dal Maso, M.; Rusanen, A.; Kerminen, V. M.; Mentel, T. F.; Wildt, J.; Kleist, E.; Kiendler-Scharr, A.; Tillmann, R.; Ehn, M.; Kulmala, M.; Boy, M. Modelling the contribution of biogenic volatile organic compounds to new particle formation in the Julich plant atmosphere chamber. *Atmos. Chem. Phys.* **2015**, *15*, 10777−10798.

(19) Jonsson, A. M.; Hallquist, M.; Ljungstrom, E. The effect of temperature and water on secondary organic aerosol formation from ozonolysis of limonene, Δ^3-carene and α-pinene. *Atmos. Chem. Phys.* **2008**, *8*, 6541−6549.

(20) Thomsen, D.; Elm, J.; Rosati, B.; Skonager, J. T.; Bilde, M.; Glasius, M. Large discrepancy in the formation of secondary organic aerosols from structurally similar monoterpenes. *ACS Earth Space Chem.* **2021**, *5*, 632−644.

(21) Liu, J.; D'Ambro, E. L.; Lee, B. H.; Schobesberger, S.; Bell, D. M.; Zaveri, R. A.; Zelenyuk, A.; Thornton, J. A.; Shilling, J. E. Monoterpene photooxidation in a continuous-flow chamber: SOA yields and impacts of oxidants, NO_x, and VOC precursors. *Environ. Sci. Technol.* **2022**, *56*, 12066−12076.

(22) Kroll, J. H.; Ng, N. L.; Murphy, S. M.; Flagan, R. C.; Seinfeld, J. H. Secondary organic aerosol formation from isoprene photooxidation. *Environ. Sci. Technol.* **2006**, *40*, 1869−1877.
(23) Ng, N. L.; Kroll, J. H.; Chan, A. W. H.; Chhabra, P. S.; Flagan, R. C.; Seinfeld, J. H. Secondary organic aerosol formation from m-xylene, toluene, and benzene. *Atmos. Chem. Phys.* **2007**, *7*, 3909−3922.
(24) Kroll, J. H.; Ng, N. L.; Murphy, S. M.; Flagan, R. C.; Seinfeld, J. H.Secondary organic aerosol formation from isoprene photooxidation under high-NO_x conditions *Geophys. Res. Lett.* 2005; Vol. *32* DOI: 10.1029/2005GL023637.
(25) Zhao, D.; Schmitt, S. H.; Wang, M.; Acir, I.-H.; Tillmann, R.; Tan, Z.; Novelli, A.; Fuchs, H.; Pullinen, I.; Wegener, R.; Rohrer, F.; Wildt, J.; Kiendler-Scharr, A.; Wahner, A.; Mentel, T. F. Effects of NO_x and SO_2 on the secondary organic aerosol formation from photooxidation of α-pinene and limonene. *Atmos. Chem. Phys.* **2018**, *18*, 1611−1628.
(26) Kiendler-Scharr, A.; Wildt, J.; Dal Maso, M.; Hohaus, T.; Kleist, E.; Mentel, T. F.; Tillmann, R.; Uerlings, R.; Schurr, U.; Wahner, A. New particle formation in forests inhibited by isoprene emissions. *Nature* **2009**, *461*, 381−384.
(27) Draper, D. C.; Farmer, D. K.; Desyaterik, Y.; Fry, J. L. A qualitative comparison of secondary organic aerosol yields and composition from ozonolysis of monoterpenes at varying concentrations of NO_2. *Atmos. Chem. Phys.* **2015**, *15*, 12267−12281.
(28) Kurtén, T.; M?ller, K. H.; Nguyen, T. B.; Schwantes, R. H.; Misztal, P. K.; Su, L.; Wennberg, P. O.; Fry, J. L.; Kjaergaard, H. G. Alkoxy radical bond scissions explain the anomalously low secondary organic aerosol and organonitrate yields from α-pinene + NO_3. *J. Phys. Chem. Lett.* **2017**, *8*, 2826−2834.
(29) Zang, X.; Zhang, Z.; Jiang, S.; Zhao, Y.; Wang, T.; Wang, C.; Li, G.; Xie, H.; Yang, J.; Wu, G.; Zhang, W.; Shu, J.; Fan, H.; Yang, X.; Jiang, L. Aerosol mass spectrometry of neutral species based on a tunable vacuum ultraviolet free electron laser. *Phys. Chem. Chem. Phys.* **2022**, *24*, 16484−16492.
(30) Krechmer, J. E.; Day, D. A.; Jimenez, J. L. Always lost but never forgotten: gas-phase wall losses are important in all Teflon environmental chambers. *Environ. Sci. Technol.* **2020**, *54*, 12890−12897.
(31) Kleindienst, T. E.; Lewandowski, M.; Offenberg, J. H.; Jaoui, M.; Edney, E. O. Ozone-isoprene reaction: Re-examination of the formation of secondary organic aerosol *Geophys. Res. Lett.* 2007; Vol. *34* DOI: 10.1029/2006GL027485.
(32) Frisch, M. J.; T, G. W.; Schlegel, H. B.; Scuseria, G. E.; Robb, M. A.; Cheeseman, J. R.; Scalmani, G.; Barone, V.; Mennucci, B.; Petersson, G. A.; Nakatsuji, H.; Caricato, M.; Li, X.; Hratchian, H. P.; Izmaylov, A. F.; Bloino, J.; Zheng, G.; Sonnenberg, J. L.; Hada, M.; Ehara, M.; Toyota, K.; Fukuda, R.; Hasegawa, J.; Ishida, M.; Nakajima, T.; Honda, Y.; Kitao, O.; Nakai, H.; Vreven, T.; Peralta, J. E., Jr.; Ogliaro, F.; Bearpark, M.; Heyd, J. J.; Brothers, E.; Kudin, K. N.; Staroverov, V. N.; Kobayashi, R.; Normand, J.; Raghavachari, K.; Rendell, A.; Burant, J. C.; Iyengar, S. S.; Tomasi, J.; Cossi, M.; Rega, N.; Millam, J. M.; Klene, M.; Knox, J. E.; Cross, J. B.; Bakken, V.; Adamo, C.; Jaramillo, J.; Gomperts, R.; Stratmann, R. E.; Yazyev, O.; Austin, A. J.; Cammi, R.; Pomelli, C.; Ochterski, J. W.; Martin, R. L.; Morokuma, K.; Zakrzewski, V. G.; Voth, G. A.; Salvador, P.; Dannenberg, J. J.; Dapprich, S.; Daniels, A. D.; Farkas; Foresman, J. B.; Ortiz, J. V.; Cioslowski, J.; Fox, D. J. *Gaussian 16*, revision C.01; Inc.: Wallingford: CT, 2016.
(33) Jia, L.; Xu, Y. The role of functional groups in the understanding of secondary organic aerosol formation mechanism from α-pinene. *Sci. Total Environ.* **2020**, *738*, No. 139831.
(34) Zhang, X.; McVay, R. C.; Huang, D. D.; Dalleska, N. F.; Aumont, B.; Flagan, R. C.; Seinfeld, J. H. Formation and evolution of molecular products in α-pinene secondary organic aerosol. *Proc. Natl. Acad. Sci. U.S.A.* **2015**, *112*, 14168−14173.
(35) Wang, L.; Liu, Y.; Wang, L. Ozonolysis of 3-carene in the atmosphere. Formation mechanism of hydroxyl radical and secondary ozonides. *Phys. Chem. Chem. Phys.* **2019**, *21*, 8081−8091.
(36) Nizkorodov, S. A.; Laskin, J.; Laskin, A. Molecular chemistry of organic aerosols through the application of high resolution mass spectrometry. *Phys. Chem. Chem. Phys.* **2011**, *13*, 3612−3629.
(37) Atkinson, R.; Arey, J. Gas-phase tropospheric chemistry of biogenic volatile organic compounds: a review. *Atmos. Environ.* **2003**, *37*, S197−S219.
(38) Ng, N. L.; Canagaratna, M. R.; Zhang, Q.; Jimenez, J. L.; Tian, J.; Ulbrich, I. M.; Kroll, J. H.; Docherty, K. S.; Chhabra, P. S.; Bahreini, R.; Murphy, S. M.; Seinfeld, J. H.; Hildebrandt, L.; Donahue, N. M.; DeCarlo, P. F.; Lanz, V. A.; Prevot, A. S. H.; Dinar, E.; Rudich, Y.; Worsnop, D. R. Organic aerosol components observed in Northern Hemispheric datasets from aerosol mass spectrometry. *Atmos. Chem. Phys.* **2010**, *10*, 4625−4641.
(39) Loza, C. L.; Chhabra, P. S.; Yee, L. D.; Craven, J. S.; Flagan, R. C.; Seinfeld, J. H. Chemical aging of m-xylene secondary organic aerosol: laboratory chamber study. *Atmos. Chem. Phys.* **2012**, *12*, 151−167.
(40) Jimenez, J. L.; Canagaratna, M. R.; Donahue, N. M.; Prevot, A. S. H.; Zhang, Q.; Kroll, J. H.; DeCarlo, P. F.; Allan, J. D.; Coe, H.; Ng, N. L.; Aiken, A. C.; Docherty, K. S.; Ulbrich, I. M.; Grieshop, A. P.; Robinson, A. L.; Duplissy, J.; Smith, J. D.; Wilson, K. R.; Lanz, V. A.; Hueglin, C.; Sun, Y. L.; Tian, J.; Laaksonen, A.; Raatikainen, T.; Rautiainen, J.; Vaattovaara, P.; Ehn, M.; Kulmala, M.; Tomlinson, J. M.; Collins, D. R.; Cubison, M. J.; Dunlea, E. J.; Huffman, J. A.; Onasch, T. B.; Alfarra, M. R.; Williams, P. I.; Bower, K.; Kondo, Y.; Schneider, J.; Drewnick, F.; Borrmann, S.; Weimer, S.; Demerjian, K.; Salcedo, D.; Cottrell, L.; Griffin, R.; Takami, A.; Miyoshi, T.; Hatakeyama, S.; Shimono, A.; Sun, J. Y.; Zhang, Y. M.; Dzepina, K.; Kimmel, J. R.; Sueper, D.; Jayne, J. T.; Herndon, S. C.; Trimborn, A. M.; Williams, L. R.; Wood, E. C.; Middlebrook, A. M.; Kolb, C. E.; Baltensperger, U.; Worsnop, D. R. Evolution of organic aerosols in the atmosphere. *Science* **2009**, *326*, 1525−1529.
(41) Voliotis, A.; Wang, Y.; Shao, Y.; Du, M.; Bannan, T. J.; Percival, C. J.; Pandis, S. N.; Alfarra, M. R.; McFiggans, G. Exploring the composition and volatility of secondary organic aerosols in mixed anthropogenic and biogenic precursor systems. *Atmos. Chem. Phys.* **2021**, *21*, 14251−14273.
(42) Donahue, N. M.; Epstein, S. A.; Pandis, S. N.; Robinson, A. L. A two-dimensional volatility basis set: 1. organic-aerosol mixing thermodynamics. *Atmos. Chem. Phys.* **2011**, *11*, 3303−3318.
(43) Bianchi, F.; Kurten, T.; Riva, M.; Mohr, C.; Rissanen, M. P.; Roldin, P.; Berndt, T.; Crounse, J. D.; Wennberg, P. O.; Mentel, T. F.; Wildt, J.; Junninen, H.; Jokinen, T.; Kulmala, M.; Worsnop, D. R.; Thornton, J. A.; Donahue, N.; Kjaergaard, H. G.; Ehn, M. Highly oxygenated organic molecules (HOM) from gas-phase autoxidation involving peroxy radicals: a key contributor to atmospheric aerosol. *Chem. Rev.* **2019**, *119*, 3472−3509.
(44) Heinritzi, M.; Dada, L.; Simon, M.; Stolzenburg, D.; Wagner, A. C.; Fischer, L.; Ahonen, L. R.; Amanatidis, S.; Baalbaki, R.; Baccarini, A.; Bauer, P. S.; Baumgartner, B.; Bianchi, F.; Brilke, S.; Chen, D.; Chiu, R.; Dias, A.; Dommen, J.; Duplissy, J.; Finkenzeller, H.; Frege, C.; Fuchs, C.; Garmash, O.; Gordon, H.; Granzin, M.; El Haddad, I.; He, X.; Helm, J.; Hofbauer, V.; Hoyle, C. R.; Kangasluoma, J.; Keber, T.; Kim, C.; Kuerten, A.; Lamkaddam, H.; Laurila, T. M.; Lampilahti, J.; Lee, C. P.; Lehtipalo, K.; Leiminger, M.; Mai, H.; Makhmutov, V.; Manninen, H. E.; Marten, R.; Mathot, S.; Mauldin, R. L.; Mentler, B.; Molteni, U.; Mueller, T.; Nie, W.; Nieminen, T.; Onnela, A.; Partoll, E.; Passananti, M.; Petaja, T.; Pfeifer, J.; Pospisilova, V.; Quelever, L. L. J.; Rissanen, M. P.; Rose, C.; Schobesberger, S.; Scholz, W.; Scholze, K.; Sipilae, M.; Steiner, G.; Stozhkov, Y.; Tauber, C.; Tham, Y. J.; Vazquez-Pufleau, M.; Virtanen, A.; Vogel, A. L.; Volkamer, R.; Wagner, R.; Wang, M.; Weitz, L.; Wimmer, D.; Xiao, M.; Yan, C.; Ye, P.; Zha, Q.; Zhou, X.; Amorim, A.; Baltensperger, U.; Hansel, A.; Kulmala, M.; Tome, A.; Winkler, P. M.; Worsnop, D. R.; Donahue, N. M.; Kirkby, J.; Curtius, J. Molecular understanding of the suppression of new-particle formation by isoprene. *Atmos. Chem. Phys.* **2020**, *20*, 11809−11821.
(45) Gao, L.; Song, J.; Mohr, C.; Huang, W.; Vallon, M.; Jiang, F.; Leisner, T.; Saathoff, H. Kinetics, SOA yields, and chemical

composition of seconaary organic aerosol from β-caryophyllene ozonolysis with and without nitrogen oxides between 213 and 313 K. *Atmos. Chem. Phys.* **2022**, *22*, 6001−6020, DOI: 10.5194/acp-22-6001-2022.

(46) Zaveri, R. A.; Wang, J.; Fan, J.; Zhang, Y.; Shilling, J. E.; Zelenyuk, A.; Mei, F.; Newsom, R.; Pekour, M.; Tomlinson, J.; Comstock, J. M.; Shrivastava, M.; Fortner, E.; Machado, L. A. T.; Artaxo, P.; Martin, S. T. Rapid growth of anthropogenic organic nanoparticles greatly alters cloud life cycle in the Amazon rainforest. *Sci. Adv.* **2022**, *8*, No. eabj0329.

(47) Cheng, X.; Chen, Q.; Li, Y. J.; Zheng, Y.; Liao, K.; Huang, G. Highly oxygenated organic molecules produced by the oxidation of benzene and toluene in a wide range of OH exposure and NO_x conditions. *Atmos. Chem. Phys.* **2021**, *21*, 12005−12019, DOI: 10.5194/acp-21-12005-2021.

(48) Kurtén, T.; Rissanen, M. P.; Mackeprang, K.; Thornton, J. A.; Hyttinen, N.; Jorgensen, S.; Ehn, M.; Kjaergaard, H. G. Computational study of hydrogen shifts and ring-opening mechanisms in α-pinene ozonolysis products. *J. Phys. Chem. A* **2015**, *119*, 11366−11375.

(49) Iyer, S.; Rissanen, M. P.; Valiev, R.; Barua, S.; Krechmer, J. E.; Thornton, J.; Ehn, M.; Kurten, T. Molecular mechanism for rapid autoxidation in α-pinene ozonolysis. *Nat. Commun.* **2021**, *12*, No. 878.

https://doi.org/10.1021/acsearthspacechem.4c00159
ACS Earth Space Chem. 2024, 8, 1668−1679